Materials Letters 186 (2017) 116–118

Contents lists available at ScienceDirect

Materials Letters

journal homepage: www.elsevier.com/locate/matlet

Atomistic simulations of grain boundary energies in tungsten

Sutatch Ratanaphan[a,*], Theerayut Boonkird[b], Rajchawit Sarochawikasit[c], Hossein Beladi[d], Katayun Barmak[e], Gregory S. Rohrer[f]

[a] Department of Tool and Materials Engineering, King Mongkut's University of Technology Thonburi, 126 Pracha Uthit Rd, Thung Khru, Bangkok 10140, Thailand
[b] Royal Thai Naval Academy, 204 Sukhumvit Road, Samut Prakan 10270, Thailand
[c] Department of Computer Engineering, King Mongkut's University of Technology Thonburi, 126 Pracha Uthit Rd, Thung Khru, Bangkok 10140, Thailand
[d] Institute for Frontier Materials, Deakin University, Geelong VIC 3216, Australia
[e] Department of Applied Physics and Applied Mathematics, Columbia University, 500 W. 120th St., New York, NY 10027, USA
[f] Department of Materials Science and Engineering, Carnegie Mellon University, Pittsburgh, PA 15213-3890, USA

ARTICLE INFO

Keywords:
Grain boundary structure
Grain boundary energy
Atomistic simulation
Nanocrystalline tungsten

ABSTRACT

The energies of grain boundaries in tungsten were calculated using embedded atom method simulations. The energies of 408 boundaries with 80 different misorientations, and a range of different boundary plane orientations, were calculated. The boundary energy depended on the lattice misorientation and the plane orientation. A comparison between the calculated boundary energy and the measured boundary population in nanocrystalline tungsten revealed that the boundary energy and population are inversely correlated. This inverse relationship reported here for this nanocrystalline metal is consistent with the Boltzmann-like distribution between grain boundary population and energy reported for metals and ceramics with microcrystalline grains.

1. Introduction

Body-centered cubic (BCC) tungsten has a wide range of applications because of its excellent hardness, thermal conductivity, and irradiation resistance [1]. Because the grain boundaries in a polycrystal influence its properties, we would like to know the types of grain boundaries that occur in tungsten, and if the relative populations can be predicted based on their energies. The grain boundary character distribution (GBCD), which describes the relative areas of grain boundaries in polycrystals as a function of lattice misorientation and grain boundary plane orientation, is known to influence grain boundary related materials properties [2]. Because the GBCD is known to be inversely correlated to the grain boundary energy distribution (GBED) in a wide range of materials [3–12], it can be hypothesized that the relative areas of grain boundaries in tungsten follow a similar trend.

To investigate this, it is necessary to know the energies of a sufficient number of grain boundaries. The distribution of grain boundary energies over all five crystallographic parameters has been measured for selected materials [6–9], but data is not currently available for tungsten. Therefore, in this work, we take the approach of computing a large number of tungsten grain boundary energies using atomistic simulations. There have been computational studies of grain boundary energies in tungsten [13,14]. However, only a limited number of boundaries were considered in these studies. The main purpose of this paper is to report the energies of 408 distinct grain boundaries in tungsten computed using the embedded-atom method. A secondary objective of this study is to investigate the relationship between the grain boundary energies and the relative areas of grain boundaries in the nanocrystalline tungsten [15]. While the inverse correlations between the grain boundary energy and the grain boundary population have been reported for many microcrystalline materials [5–11], it is not yet known if nanocrystalline materials will have the same property.

2. Method

To survey a large number of grain boundary energies in tungsten, we constructed grain boundaries in periodic boxes with a minimum length of $17a_0/2$ in the y and z directions and with a dimension less than or equal to $20a_0/2$ in the x direction, where a_0 is the lattice spacing. There were 408 boundaries with 80 different misorientations that could be represented in this volume. The set of boundaries and the computational scheme were identical to the previous simulations of grain boundary energies in BCC metals [16]; these methods were

* Corresponding author.
E-mail address: sutatch.ratanaphan@mail.kmutt.ac.th (S. Ratanaphan).

http://dx.doi.org/10.1016/j.matlet.2016.09.104
Received 24 August 2016; Accepted 25 September 2016
Available online 28 September 2016
0167-577X/

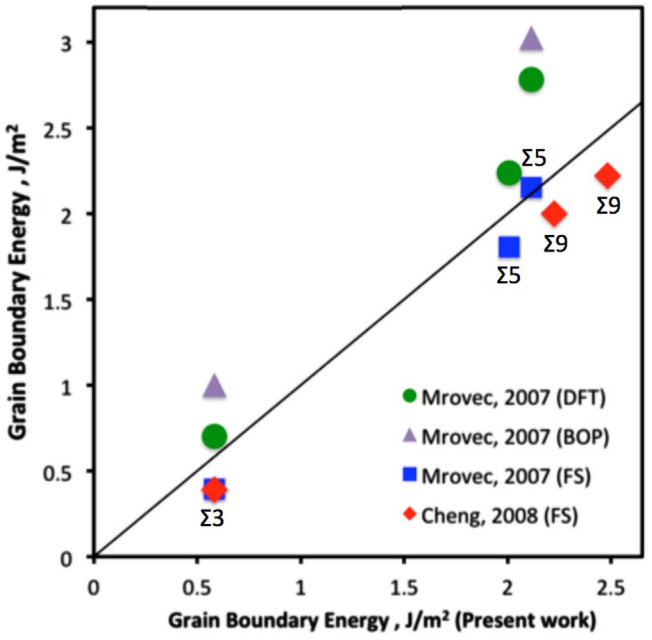

Fig. 1. Comparisons between the present and the previous grain boundary energies calculated using a density functional theory (DFT), a bond-order potential (BOP) and a Finnis-Sinclair (FS) potential [13,14]. The solid line represents a unit slope.

derived from similar studies of face-centered cubic (FCC) metals [17,18]. The Zhou potential [19] was used in this study. The relative areas of grain boundaries were derived from transmission electron microscopy orientation maps using a stereological method [20]. The details of the sample preparation and grain boundary distribution analysis were published previously [15,21].

3. Result and discussion

Grain boundary energies calculated in the present study are compared to the results of previous studies in Fig. 1. [13,14]. While the grain boundary energies calculated using density functional theory (DFT), a bond-order potential (BOP) and a Finnis-Sinclair (FS) potential are different, the relative grain boundary energies in each computational scheme are linearly correlated to the present simulated grain boundary energies..

We compared the energies of 408 distinct grain boundaries to the measured grain boundary population in the nanocrystalline tungsten [15] (Fig. 2). The most frequently observed boundary in the plot is the Σ3 (321) symmetrical tilt boundary, 3.3 MRD, which has a slightly larger population than the coherent twin boundary, 2.9 MRD. The (110) symmetrical boundaries are not only frequently observed but also have low energies. The relative area of a grain boundary in nanocrystalline tungsten is highly correlated to the grain boundary energy (correlation coefficient =−0.7) in a similar manner to what has been previously reported for microcrystalline materials [5–10]..

The GBEDs and GBCDs for the Σ3 and Σ9 misorientations are shown in Fig. 3. The distribution of grain boundary energy at the Σ3 (Fig. 3b) is strongly dependent on the boundary plane orientation, which agrees with previous studies [16]. For Σ3, the (111) twist boundary, marked with a triangle in Fig. 3a, has the maximum energy (2.503 J/m^2). The coherent twin boundary has the minimum boundary energy (0.582 J/m^2) of all 408 boundaries considered. While this is the minimum energy, other tilt boundaries on the same great circle also have relatively low energies (less than 1 J/m^2, Fig. 2). The grain boundary plane distribution at the Σ3 (Fig. 3**c**) maximizes along the zone of tilt boundaries perpendicular to [111] at about ~ 3 MRD. This indicates that the populations of these boundaries are about three times greater than expected in a random distribution. The results show

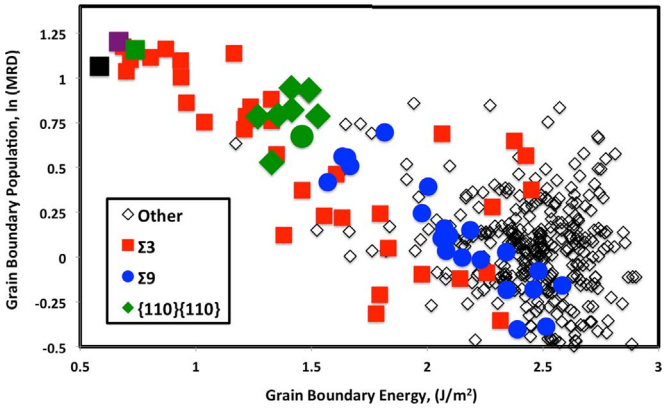

Fig. 2. The relationship between the simulated grain boundary energies in tungsten and the measured grain boundary populations in nanocrystalline tungsten [15]. The grain boundaries are separated into four categories, Σ3 (squares), Σ9 (circles), and symmetrical {110}{110}(green), and other (diamonds). The Σ3 (211) symmetrical tilt boundary (the coherent twin boundary) and the Σ3 (321) symmetrical tilt boundary are colored black and purple respectively. (For interpretation of the references to color in this figure legend, the reader is referred to the web version of this article.)

that the highly populated grain boundaries at the Σ3 correspond to low energy boundaries (Fig. 3b)..

The distribution of grain boundary energy at the Σ9 is shown in Fig. 3e. The distributions of simulated grain boundary energies at the Σ3 and Σ9 are consistent with the previously simulated grain boundary energies in iron [12,22], molybdenum [16], and the measured boundary energy in iron [9]. While the energy of the coherent twin boundary in tungsten (0.582 J/m^2) is significantly larger than the same boundary in molybdenum (0.389 J/m^2) and iron (0.262 J/m^2), the ratios of the coherent twin boundary energy to the average boundary energy in tungsten (25%), molybdenum (25%), and iron (24%) are similar [16]. The maximum grain boundary population at the Σ9 is centered at the (110) twist boundary and has a value of 2.0 MRD (Fig. 3f). The minima in the distribution are located along the zone of tilt boundaries, which are high energies (Fig. 3e). Based on the grain boundary population and energy distributions at the Σ3 and Σ9, it is clear that those grain boundaries with lower (higher) energies have higher (lower) population. It should be noted that the ratios of the coherent twin boundary energies to the average boundary energies in the BCC metals (~25%) are much larger than those in the FCC metals, which are: copper (3%), gold (6%), nickel (6%) and aluminum (14%) [18]. If the inverse relationship between the grain boundary population and energy is influenced by the magnitude of the energy difference between the boundary with the minimum energy (the twin) and the average, then it would follow that the twin populations in BCC metals would be significantly lower than the populations in FCC metals.

4. Summary

In this study, we computed the energies of 408 boundaries in tungsten using the embedded atom method. The simulated grain boundary energies were strongly influenced by the orientation of the grain boundary plane. The grain boundary population distribution in nanocrystalline tungsten was inversely correlated to the simulated grain boundary energy. This inverse relationship suggests a Boltzmann-like distribution between grain boundary energy and population, which is consistent with previous observations of microcrystalline materials.

Acknowledgments

This work was supported by Research Strengthening Project of the Faculty of Engineering, King Mongkut's University of Technology Thonburi. The authors also acknowledge the National Research

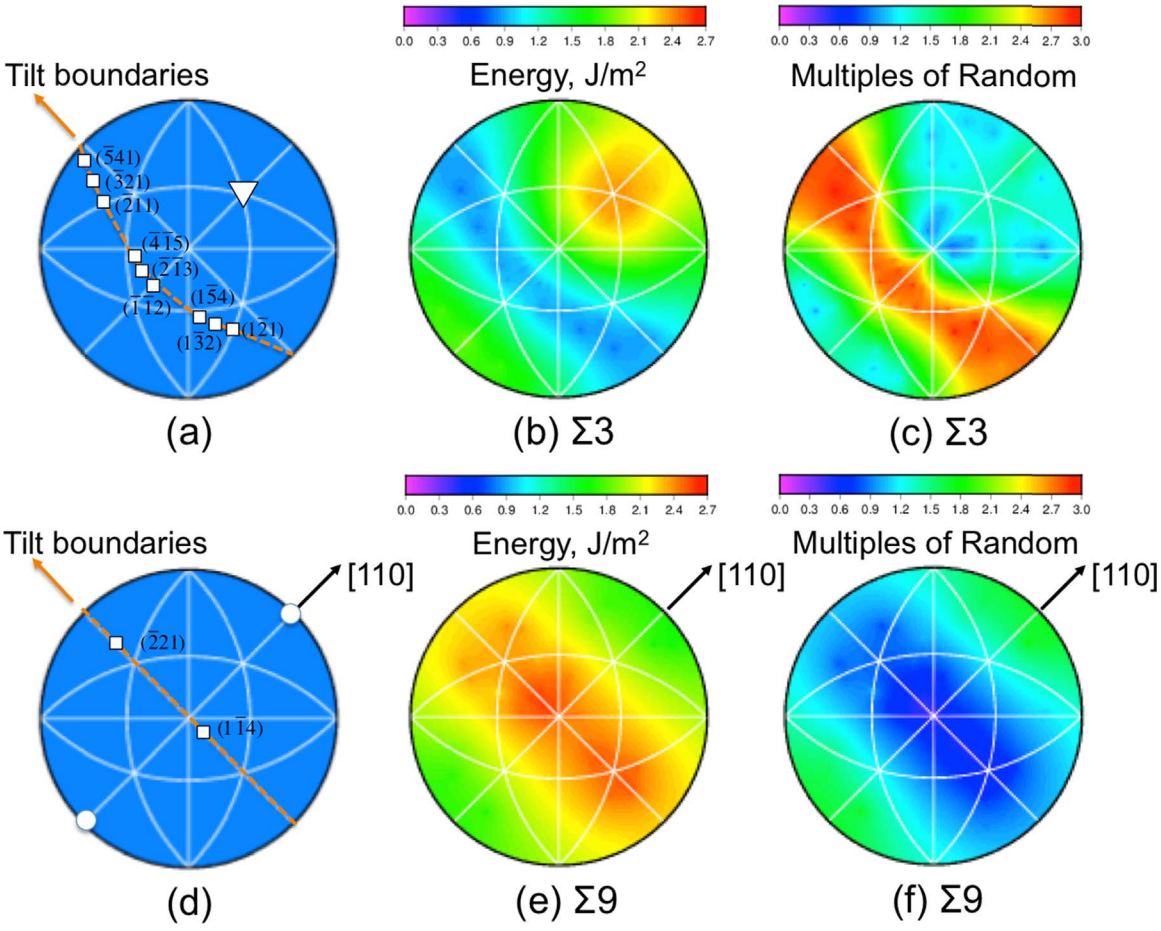

Fig. 3. Schematic representation of symmetric tilt boundaries at Σ3, 60°/[111] (a) and Σ9, 39°/[110] (d). The symmetric (111) twist boundary and the symmetric <110> twist boundary are marked with a triangle and circles respectively. The distributions of calculated grain boundary energy for Σ3 (b) and Σ9 (e) are plotted on a stereographic projection. Using data from reference [15], the grain boundary character distribution for Σ3 (c) and Σ9 (f) are plotted with units of multiples of a random distribution (MRD).

University of Thailand, Office of the Higher Education Commission. We are also grateful to Dr. David Olmsted for the code used for grain boundary energy calculation.

Appendix A. Supporting information

Supplementary data associated with this article can be found in the online version at doi:10.1016/j.matlet.2016.09.104.

References

[1] S. Wurster, R. Pippan, Scr. Mater. 60 (2009) 1083–1087.
[2] C.-S. Kim, A.D. Rollett, G.S. Rohrer, Scr. Mater. 54 (2006) 1005–1009.
[3] D.M. Saylor, A. Morawiec, G.S. Rohrer, J. Am. Ceram. Soc. 85 (2002) 3081–3083.
[4] E.A. Holm, G.S. Rohrer, S.M. Foiles, A.D. Rollett, H.M. Miller, D.L. Olmsted, Acta Mater. 59 (2011) 5250–5256.
[5] G.S. Rohrer, E.A. Holm, A.D. Rollett, S.M. Foiles, J. Li, D.L. Olmsted, Acta Mater. 58 (2010) 5063–5069.
[6] J. Li, S.J. Dillon, G.S. Rohrer, Acta Mater. 57 (2009) 4304–4311.
[7] H. Beladi, N.T. Nuhfer, G.S. Rohrer, Acta Mater. 70 (2014) 281–289.
[8] D.M. Saylor, A. Morawiec, G.S. Rohrer, Acta Mater. 51 (2003) 3675–3686.
[9] H. Beladi, G.S. Rohrer, Acta Mater. 61 (2013) 1404–1412.
[10] S. Ratanaphan, Y. Yoon, G.S. Rohrer, J. Mater. Sci. 49 (2014) 4938–4945.
[11] J. Gruber, D.C. George, A.P. Kuprat, G.S. Rohrer, A.D. Rollett, Scr. Mater. 53 (2005) 351–355.
[12] H. Beladi, G.S. Rohrer, Metall. Mater. Trans. A 44 (2012) 115–124.
[13] Y. Cheng, M. Mrovec, P. Gumbsch, Philos. Mag. 88 (2008) 547–560.
[14] M. Mrovec, R. Gröger, A.G. Bailey, D. Nguyen-Manh, C. Elsässer, V. Vitek, Phys. Rev. B 75 (2007) 104119.
[15] X. Liu, D. Choi, H. Beladi, N.T. Nuhfer, G.S. Rohrer, K. Barmak, Scr. Mater. 69 (2013) 413–416.
[16] S. Ratanaphan, D.L. Olmsted, V.V. Bulatov, E.A. Holm, A.D. Rollett, G.S. Rohrer, Acta Mater. 88 (2015) 346–354.
[17] D.L. Olmsted, S.M. Foiles, E.A. Holm, Acta Mater. 57 (2009) 3694–3703.
[18] E.A. Holm, D.L. Olmsted, S.M. Foiles, Scr. Mater. 63 (2010) 905–908.
[19] X.W. Zhou, H.N.G. Wadley, R.A. Johnson, D.J. Larson, N. Tabat, A. Cerezo, A.K. Petford-Long, G.D.W. Smith, P.H. Clifton, R.L. Martens, T.F. Kelly, Acta Mater. 49 (2001) 4005–4015.
[20] D.M. Saylor, B.S. El-Dasher, B.L. Adams, G.S. Rohrer, Metall. Mater. Trans. A 35 (2004) 1981–1989.
[21] D. Choi, B. Wang, S. Chung, X. Liu, A. Darbal, A. Wise, N.T. Nuhfer, K. Barmak, A.P. Warren, K.R. Coffey, M.F. Toney, J. Vac. Sci. Technol. A 29 (2011) 51512.
[22] H.-K. Kim, W.-S. Ko, H.-J. Lee, S.G. Kim, B.-J. Lee, Scr. Mater. 64 (2011) 1152–1155.